



OPEN

Evaluating cutinase from *Fusarium oxysporum* as a biocatalyst for the degradation of nine synthetic polymer

Maycon Vinicius Damasceno de Oliveira^{ID 1}, Gabriel Calandrini^{ID 2}✉, Cláuber Henrique Souza da Costa^{ID 3}, Carlos Gabriel da Silva de Souza^{ID 1}, Cláudio Nahum Alves¹, José Rogério A. Silva^{ID 1,4}, Anderson H. Lima^{ID 1} & Jerônimo Lameira^{ID 1}✉

Plastic poses a significant environmental impact due to its chemical resilience, leading to prolonged and degradation times and resulting in widespread adverse effects on global flora and fauna. Cutinases are essential enzymes in the biodegradation process of synthetic polymers like polyethylene terephthalate (PET), which recognized organisms can break down. Here, we used molecular dynamics and binding free energy calculations to explore the interaction of nine synthetic polymers, including PET, with Cutinase from *Fusarium oxysporum* (*FoCut*). According to our findings, the polymers poly(ethylene terephthalate) (PET), poly(3-hydroxybutyrate-co-3-hydroxyhexanoate) (PHBH), poly(butylene succinate) (PBS), poly(butylene adipate-co-terephthalate) (PBAT) and poly(ϵ -caprolactone) (PCL) can bind to the Cutinase enzyme from *F. oxysporum*, indicating potential biodegradation activity for these polymers. PET exhibited the highest binding affinity (~ 34.26 kcal/mol). Besides PET, the polymers PHBH, PBS, PBAT, and PCL also demonstrated significant affinities for the *FoCut* enzyme, with binding values of ~ 18.44, ~ 29.71, ~ 22.78, and ~ 22.26 kcal/mol, respectively. Additionally, analysis of the phylogenetic tree of cutinases produced by different organisms demonstrated that even though the organisms belong to different kingdoms, the cutinase from *F. oxysporum* (*FoCut*) showed biological similarity in its activity in degrading polymers with the cutinase enzyme from the bacterium *Kineococcus radiotolerans* and the fungus *Moniliophthora roreri*. Furthermore, the phylogenetic analysis demonstrated that the PETase enzyme has a very high similarity with the bacterial cutinase enzyme than with the fungal cutinase, therefore demonstrating that the PETase enzyme from *Ideonella sakaiensis* can easily be a modified bacterial cutinase enzyme that created a unique feature in biodegrading only the pet polymer through an evolutionary process due to its environment and its biochemical need for carbon. Our data demonstrate that bacterial cutinase enzymes have the same common ancestor as the PETase enzyme. Therefore, cutinases and PETase are interconnected through their biological similarity in biodegrading polymers. We demonstrated that important conserved regions, such as the Ser-Asp-His catalytic triad, exist in the enzyme's catalytic site and that all Cut enzymes from different organisms have the same region to couple with the polymer structures.

Keywords Cutinase, Polymer, *Fusarium oxysporum*, Molecular dynamic, Phylogentic

Plastics are essential materials for modern society due to their distinct properties, including lightness, durability, versatility, and low production costs^{1–3}. However, their non-degradability poses a significant threat to the environment, primarily because synthetic polymers are chemically resistant and take a long time to degrade,

¹Laboratório de Planejamento e Desenvolvimento de Fármacos, Instituto de Ciências Exatas e Naturais, Universidade Federal do Pará, Belém, Pará 66075-110, Brazil. ²Núcleo de Ecologia Aquática e Pesca (NEAP), Universidade Federal do Pará, Belém, Pará 66075-110, Brazil. ³Center for Computing in Engineering & Sciences, IQ/UNICAMP, Campinas, Brazil. ⁴Catalysis and Peptide Research Unit, University of KwaZulu-Natal, Durban 4000, South Africa. ✉email: gabriel.calandrini@icb.ufpa.br; lameira@ufpa.br

Usual Name	2D structure	Cutinase organism with degradation activity	Ref
PET		<i>F. oxysporum</i> ; <i>M. roreri</i> ; <i>T. fuscum</i> ; <i>T. cellulosilytica</i> ; <i>T. alba</i> ; <i>S. viridis</i> ; <i>H. insolens</i>	12-17, 54
		<i>T. alba</i>	19
PLA			18
PHB			55
PHBH			—
PHBV		<i>T. cellulosilytica</i>	20
PBS		<i>E. solani</i> ; <i>T. cellulosilytica</i> ; <i>A. oryzae</i> ; <i>M. cinnamomea</i> ; <i>H. insolens</i>	20, 21, 43, 56, 57

Continued

Usual Name	Polymers 2D structure	Cutinase organism with degradation activity	Ref
PBAT		<i>F. solani</i> ; <i>T. fusca</i> ; <i>H. insolens</i>	22,23,57
PCL		<i>M. roreri</i> ; <i>F. solani</i> ; <i>K. radiotolerans</i> ; <i>A. oryzae</i> ; <i>M. cinnamomea</i> ; <i>H. insolens</i> ; <i>F. vanettei</i>	12,18,43,55–58
PES		<i>M. roreri</i> ; <i>F. solani</i>	12,59

Table 1. Two-dimensional structure and name of each of the nine selected polymers and works that demonstrated the Cut enzyme from different organisms degrading the polymer.

remaining for years, especially in oceans⁴. The use of biodegradable polymers, both synthetic and natural, has emerged as a more sustainable alternative for plastic production, since pollution by non-biodegradable plastics affects everything from marine animals, interfering with their feeding behaviour, to humans with the presence of microplastics^{5–7}. The biodegradation of polymers occurs through the activity of enzymes produced by microorganisms such as fungi and bacteria, capable of secreting enzymes such as PETases and Cutinases^{8,9}.

Cutinases (Cut), a type of serine hydrolase found in various organisms (e.g. *Fusarium solani pisi*¹⁰, *Fusarium oxysporum*¹¹, *Moniliophthora roreri*¹², *Saccharomonospora viridis*¹³, *Thermobifida alba*¹⁴, *Thermobifida cellullosilytica*¹⁵, *Thermobifida fusca*¹⁶, *Humicola insolens*¹⁷, *Kineococcus radiotolerans*¹⁸), are capable of degrading cutin, a fatty acid polyester that forms the main component of plant cuticles. These enzymes have emerged as vital biocatalysts in the breakdown of synthetic polymers such as poly(ethylene terephthalate) (PET)¹², poly(lactic Acid) (PLA)¹⁹, poly(3-hydroxybutyrate-co-3-hydroxyvalerate) (PHBV)²⁰, poly(butylene succinate) (PBS)²¹, poly(butylene adipate-co-terephthalate) (PBAT)^{22,23}, poly(ϵ -caprolactone) (PCL)¹², poly(ethylene succinate) (PES)¹². In 2022, Abokitse et al. demonstrated that the bacterium *Kineococcus radiotolerans* also produces a Cut capable of biodegrading polymers. Notably, *F. oxysporum* has so far only shown PET biodegradation activity among polymers.

The fungus *Fusarium oxysporum* is known to thrive in moist, warm environments. However, *Fusarium* genus can be quite versatile and adapt to a various environmental conditions, including dry conditions or aquatic habitats in certain cases^{24,25}. In the Amazon, for example, the fungus is the leading cause of the death of black pepper plantations in Pará²⁶. Pará is one of the primary producers and exporters of black pepper in Brazil²⁷. Therefore, *F. oxysporum*, in addition to being a problem in the health sector as it causes the disease fusariosis, is also a problem for the economic sector of a region²⁴. Furthermore, this organism attacks other crops such as bananas²⁸ and tomatoes²⁹.

Therefore, this work evaluates synthetic polymers' binding affinity the *Fusarium oxysporum* Cutinase (Cut) enzyme using computational methods such as Molecular Dynamics, Molecular Docking, and Binding Free Energy calculations, as employed in previous studies^{30–35}. Overall, we provide insights into the potential use of this enzyme as a biocatalyst in the biodegradation of polymers other than PET.

Material and methods

Phylogenetic analysis protocol

We used the Molecular Evolutionary Genetics Analysis version 11 (MEGA11)³⁶ software. We selected some organisms that produce the Cut enzyme, fungi, and bacteria deposited in the PDB. We selected the FASTA sequence from the PDB of these Cut proteins as *Halopseudomonas bauzanensis* (8AIT)³⁷, *Fusarium oxysporum* (5AJH)¹¹, *Fusarium vanettenii* (1CEX)³⁸, *Fusarium solani* (1CUS)³⁹, *Paraphoma* sp. (7CY3), *Humicola insolens* (4OYY)⁴⁰, *Colletotrichum gloeosporioides* (3DCN)⁴¹, *Aspergillus oryzae* (3GBS)⁴², *Malbranchea cinnamomea* (5X88)⁴³, *Trichoderma reesei* (4PSC)⁴⁴, *Saccharomonospora viridis* (4WFI)⁴⁵, *Saccharopolyspora flava* (7QJP)⁴⁶, *Thermobifida cellullosilytica* (5LUI)⁴⁷, *Thermobifida fusca* (5ZOA), *Thermobifida alba* (3VIS)⁴⁸. Two organisms were selected from recent studies and do not have the crystallized structure of the Cut enzyme deposited in the PDB, namely *Moniliophthora roreri* (GenBank: ESK97883.1)¹² and *Kineococcus radiotolerans* (GenBank: ABS05574.1)¹⁸. Additionally, we added the PETase enzyme from the bacteria *Ideonella sakaiensis* (6EQE)¹. We performed a global alignment of the sequences using ClustalW. The phylogenetic tree was plotted using the Neighbor-Joining statistical method, using Bootstrap method with 10,000 replications.

Structural preparation of polymers and FoCut

The three-dimensional structure of the Cutinase hydrolase from *Fusarium oxysporum* (FoCut) was acquired from the RCSB Protein Data Bank⁴⁹ using the PDB code 5AJH¹¹. This structure was determined by X-ray diffraction with a resolution of 1.90 Å. The nine polymer structures were designed in 2D (Table 1) using the MarvinSketch⁵⁰ program (version 18.9) and subsequently converted and analyzed in the 3D model using the Avogadro⁵¹ program (version 1.2.0). The PET, PLA, PHB, PBS, PCL and PES structures were used a tetramer. PHBH and PHBV structure were used as a dimer. PBAT structure was used as a monomer. This difference of each ligand (tetramer, dimer or monomer) is related to the volume of each structure. Finally, 3D structures were optimized in the Gaussian09⁵² program using the Hartree-Fock⁵³ method with the 6-31G* basis set.

Docking molecular protocol

We used the Molegro Virtual Docker (MVD) software (version 5.5)⁶⁰ for the molecular docking stage. MVD employs the MolDock heuristic search algorithm, which uses a piecewise linear potential (PLP) scoring function that includes hydrogen and electrostatic interaction terms⁶⁰. Molecular docking was performed using a flexible docking approach⁶¹, where the active site residues of FoCut were considered flexible to ensure optimal coupling with the nine polymer structures. This strategy allowed for more interactions at the enzyme site, eliminating the need to apply a restriction force to maintain these interactions during the Molecular Dynamics step. Then, for the molecular docking protocol, we used the MolDock SE algorithm with the following parameters: number of runs = 10, space coordinates (X = - 15.35, Y = 13.52, Z = - 41.65), maximum iterations = 1500, maximum population size = 50, and grid resolution = 25.0 Å.

Molecular Dynamics (MD) protocol

Initially, we used the PROPKA⁶² to determine the protonation states of the ionizable residues of FoCut. The nine polymers and the protein were submitted to the CHARMM-GUI web server using the CHARMM36 force field^{63–65}, as applied in our previous work³⁴. The systems were solvated with water molecules using the TIP3P explicit solvation model⁶⁶, within an octahedral box, with a radius of 12.0 Å (distance from the protein to the box), and Cl⁻ counter-ions to maintain the electroneutrality of the system. We prepared nine complexes: PEP-,

PLA-, PHB-, PHBH-, PHBV-, PBS-, PBAT-, PCL-, PES-*FoCut*. Then, the structural-energetic minimization step was performed in four stages. In the first step, we included only the counter-ions and water molecules. In the second step, we minimized only the hydrogen atoms of the protein structure. The third step included the hydrogen atoms of the entire complex (ligand–protein structure and water molecules). The final step involved minimizing the entire system. Then, all the systems were subjected to a heating step from 0 to 300 K using 200 ps of MD in a constant volume with a restraint weight of 5.0 kcal·mol⁻¹·Å² at the positions of the atoms (complex). Subsequently, all systems were equilibrated with 500 ps of MD with no restraints at a constant pressure of 1 bar. The temperature of the systems was maintained at 300 K using a Langevin thermostat with a collision frequency of 2 ps⁻¹, and the isotropic constant pressure was maintained at 1 bar using a Berendsen barostat. We used a cutoff of 10 Å for non-bonded interactions and the Particle Mesh Ewald (PME) method to calculate long-range electrostatic interactions. MD simulations were performed assuming a simulation time of 300 ns, conducted in triplicate (100 ns for each replicate). All MM simulations were carried out in AMBER20⁶⁷ package. Additionally, we performed an MD simulation of *FoCut* without any polymer, assuming a simulation time of 1 μs.

Binding free energy calculations and per-residue free energy decomposition protocol

To evaluate the affinity of the nine polymers to *FoCut*, we employed the Molecular Mechanics with Generalized Born and Surface Area Solvation (MM/GBSA) approach^{68,69} available in Amber20⁶⁷. We selected 10,000 frames from the MD trajectory, corresponding to the entire 100 ns simulation of each replicate, to evaluate the contributions and the binding free energy ($\Delta G_{binding}$) values throughout the simulation time. Subsequently, we performed a decomposition analysis to identify the central residues that contribute to the binding affinity of the polymer–*FoCut* complex.

The $\Delta G_{binding}$ is calculated through Eq. 1, where the terms ΔE_{MM} , ΔG_{sol} and $T\Delta S$ represent the changes in the molecular mechanical energy of the gas phase (MM), free solvation energy, and conformational entropy after the binding state of the binder, respectively^{31,69–71}.

$$\Delta G_{binding} = \Delta E_{MM} + \Delta G_{sol} - T\Delta S \quad (1)$$

Therefore, ΔE_{MM} refers to the energy of molecular mechanics which can be described as the sum of intramolecular energy (internal, electrostatic and van der Waals energy)^{31,69–71}. ΔG_{sol} represents the sum of all the electrostatic solvation energy (polar contribution) and all the nonpolar contribution between the solute and the solvent and right after the third term of the $\Delta G_{binding}$ equation, $T\Delta S$, represents the temperature, T , and entropy, ΔS , of the system⁷². In addition, the GB method has limitations in calculating entropy because, due to the high computational cost, changes in conformational entropy are ignored mainly since only the relative binding free energies of similar ligands are needed⁷².

Results and discussion

Phylogenetic analysis of organisms that produce Cutinases

The phylogenetic tree (Fig. 1) was developed from the alignment of cutinases present in 17 different organisms to evaluate the similarity of cutinases produced between species compared to cutinases already described in the literature as biodegrading polymers, such as *Aspergillus oryzae*, *Moniliophthora roreri*, *Paraphoma* sp., *Hemicola insolens*, *Saccharomonospora viridis*, *Thermobifida fusca*, *Fusarium solani*, among others^{12,17,23,73–76}.

The analysis of the phylogenetic tree showed the lineages of several organisms, both fungi and bacteria, that can produce the cutinase enzyme. Among the fungi, the species *Fusarium oxysporum* stands out, being the species studied in this work, belonging to the same genus as the species *F. solani* and *F. vanettenii*, which can be pathogenic to both plants and humans, causing diseases on plants' roots and several diseases in humans such as pneumonia and other consequences due to contamination by toxins produced by the fungi^{77–79}.

Among the bacteria, the genus *Thermobifida*, which are thermophilic bacteria capable of adapting to environments with high temperatures and have great potential for biodegradation, the species *Thermobifida fusca* is widely used in studies of cutinase production for biodegradation of polyethylene terephthalate¹⁶ tag. The species forms a clade with the species *T. cellulosilytica* and *T. alba* and are evolutionarily distant from the fungal species of the *Fusarium*.

The bacterial species *Ideonella sakaiensis* was also analyzed, and the organism is phylogenetically distinct from other cutinase-producing bacteria, but closer to other species as *Halopseudomonas bauzanensis* and *Kineococcus radiotolerans*. However, its grouping with those other bacteria may be due to a shared ability to degrade synthetic polymers, as *I. sakaiensis* produces the PETase enzyme.

Cutinases and PETases are distinct enzymes, but share similar catalytic mechanisms, which may indicate that the enzymes belong to the same family of cutinases⁸⁰. Furthermore, the phylogenetic analysis revealed that the PETase enzyme shares more similarity with bacterial cutinases than fungal cutinases. Moreover, Yoshida et al.⁸¹ and Maity et al.⁸² indicated a significant similarity (> 52%) of the PETase enzyme with the cutinases produced by the thermophilic bacterium *Thermobifida fusca*. This suggests that the PETase enzyme from *Ideonella sakaiensis* likely evolved from a bacterial cutinase, acquiring a unique ability to specifically degrade PET polymers through an evolutionary process driven by environmental pressures and the organism's biochemical need for carbon as a source of energy^{1,80}. Another point in PETase, this enzyme retains the ancestral fold of the α/β-hydrolase. However, unlike homologous cutinases, its active site is more favourable for the entry of the PET polymer since the active site cleft is in a more open form than in cutinases, which This is traumatic since the PETase enzyme has a high ability to degrade PET, demonstrated in computational and experimental studies^{1,34,81,83–85}.

Our phylogenetic tree data indicate that the similarity between the genetic sequences of PETase and Cutinase is supported by enzymatic engineering¹. We demonstrated that a mutant version of the PETase enzyme, after introducing a double mutation inspired by the cutinase from *T. fusca*¹, narrowed the binding site region for the

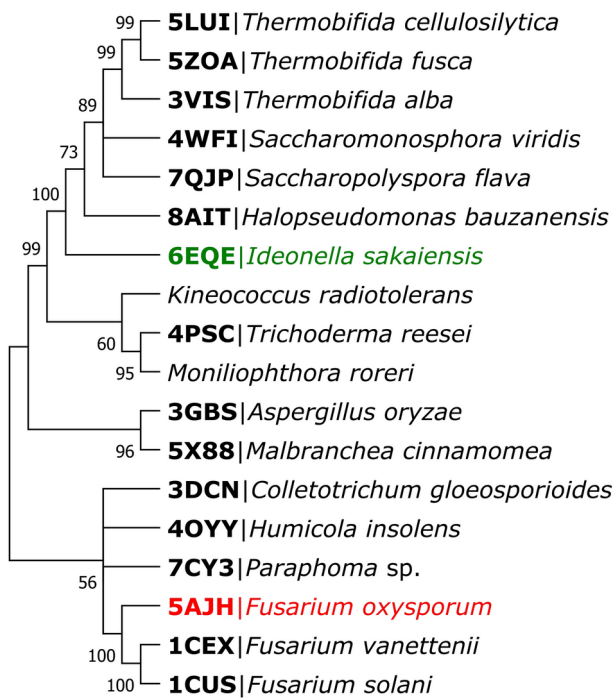


Fig. 1. Phylogenetic tree of Cutinases from different organism fungus and bacteria, highlighting the organism used in this research.

polymer, and exhibited greater affinity for PET, resulting in more efficient polymer degradation. Thus, our study broadens the possibilities for future research in protein engineering, focusing on guided mutations based on conserved regions of bacterial and fungal cutinases, aiming to enhance the catalytic activity of PETase for the degradation of PET and potentially other polymers. We established the phylogenetic similarity between PETase and bacterial cutinases and conducted a phylogenetic analysis to map cutinases experimentally confirmed to degrade synthetic polymers. Table 1 enumerates the polymers and the respective organisms either tested for degradation or demonstrated to exhibit this capability. The phylogenetic tree was examined to evaluate the proximity of these organisms and to determine the extent of similarity between the cutinase from *Fusarium oxysporum* and enzymes reported to possess polymer-degradation activity. Our findings reveal that, while the *F. oxysporum* cutinase does not exhibit a high degree of similarity to bacterial cutinases, it demonstrates considerable potential for degrading polymers beyond PET, as supported by experimental evidence (e.g., *Thermobifida fusca*, known to degrade PBAT). PET was utilized as the benchmark polymer for comparative analysis. We emphasized the structural resemblance between PETase and cutinase, particularly at their catalytic sites, illustrating that PET binds to the same region of the active site in both enzymes. This observation is significant, as both enzymes employ an identical catalytic mechanism involving the serine residue within their catalytic triad. The phylogenetic tree thus serves as a crucial framework for advancing research, facilitating the comparison of polymer-degrading organisms and investigating whether bacterial cutinases exhibit a broader capacity for synthetic polymer degradation compared to *F. oxysporum*.

The phylogenetic analysis shows that even though they are from different organisms, bacteria and fungi, these enzymes have structural similarity and, in addition, the cutinase from the bacteria *K. radiotolerans* has the same capacity to biodegrade PCL as does the cutinase from the organisms *M. roreri*, *F. solani*, *K. radiotolerans*, *A. oryzae*, *M. cinnamomea*, *H. insolens*, *F. vanettenii*^{12,18,43,55–58}. From a structural point of view, all cutinases from the 17 selected organisms have the Ser–His–Asp catalytic triad in common, in addition, they have at least one disulfide bond. Chemically and biologically, disulfide bonds can be correlated with the resistance capacity of cutinase to adverse conditions, from pH to temperature variations, showing that cutinase from different organisms that have adverse environmental conditions have different amounts of disulfide bonds between fungi and bacteria^{42,86}. The cutinase of the filamentous fungus *A. oryzae* has an additional disulfide bond, like the fungi *T. reesei* and *M. cinnamomea*, which is crucial to improving the thermal stability of AoCut in the PCL polymer biodegradation process⁴². Among the bacteria studied, the bacterium *K. radiotolerans* is the closest phylogenetically to fungi. Besides, it is also observed that bacterial cutinase has the affinity to biodegrade many more polymers other than PET—among the nine selected in this research—than fungal cutinase (Table 1).

Among the nine polymers studied, some fungal organisms are shown to be capable of biodegrading only one type of polymer. Fungi of the genus *Fusarium* are those most capable of biodegrading several synthetic polymers (such as PET, PBAT, PCL, PBS and PES) as well as *M. roreri*, which is capable of biodegrading three polymers (PET, PCL and PES) (Table 1). Phylogenetic analysis and MD simulations can be helpful for designing more active and thermostable proteins capable of degrading these polymers.

Biological similarity between PETase and FoCut

The Yoshida group showed that the bacterium *Ideonella sakaiensis* expresses two enzymes that are involved in the biodegradation of PET, the enzyme PETase and MHETase^{81,87}. This PETase enzyme catalyzes the biodegradation reaction of PET by converting it into mono(2-hydroxyethyl) terephthalic acid (MHET) and releasing bis-(hydroxyethyl) terephthalate (BHET) and terephthalic acid (TPA) as products.

In the proposed catalytic mechanism of polymer biodegradation by PETase, the carbonyl group attached to the first benzene ring is oriented toward the centre of the polymer-binding cleft, where the catalytic triad Ser160, Asp206, and His237 is located^{2,3,88}. The essential residue Ser160 is responsible for the nucleophilic attack of the enzyme on the substrate and then the ester bond is cleaved with the participation of a water molecule, similar to the mechanism of the Cutinase enzyme^{2,89}.

Here, we performed global align by ClustalW in MEGA 11³⁶ software of the enzyme PETase (PDB ID: 6EQE¹) and Cutinase (PDB ID: 5AJH¹¹) in order to identify the main conserved and semi-conserved residues (Fig. 2, panel A). Despite being from extremely different organisms, we identified that these enzymes have similarities in their structure, which provides insights into their ability to biodegrade the PET polymer. The Cutinase from *F. oxysporum* also has a catalytic triad of Ser121, Asp176 and His189 residues. Among the conserved residues are the catalytic residues of the *Is*PETase triad Ser160, Asp176 and His237 being Ser121, Asp176 and His189 for FoCut (Fig. 2, panel B and C).

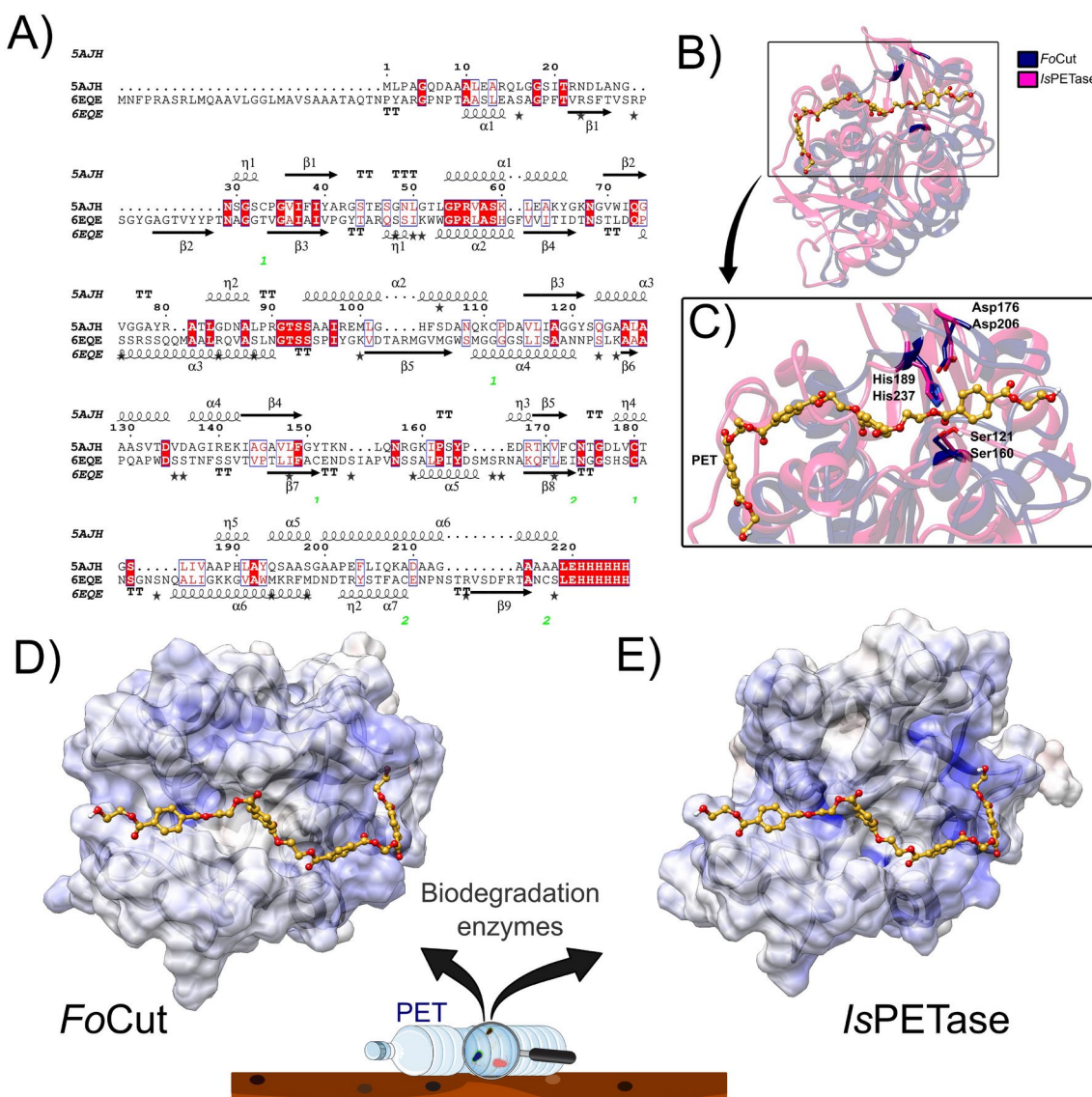


Fig. 2. Structural comparison between the enzyme *Is*PETase (PDB ID: 6EQE) and FoCut (PDB ID: 5AJH). (A) Non-conserved, conserved and semi-conserved residues observed in the global alignment by ClustalW, (B) overlap of the enzymes with the structure of the PET tetramer present in the catalytic site of the enzyme, (C) region of the catalytic triad in comparison for both enzymes, binding pocket for enzyme (D) FoCut and (E) *Is*PETase.

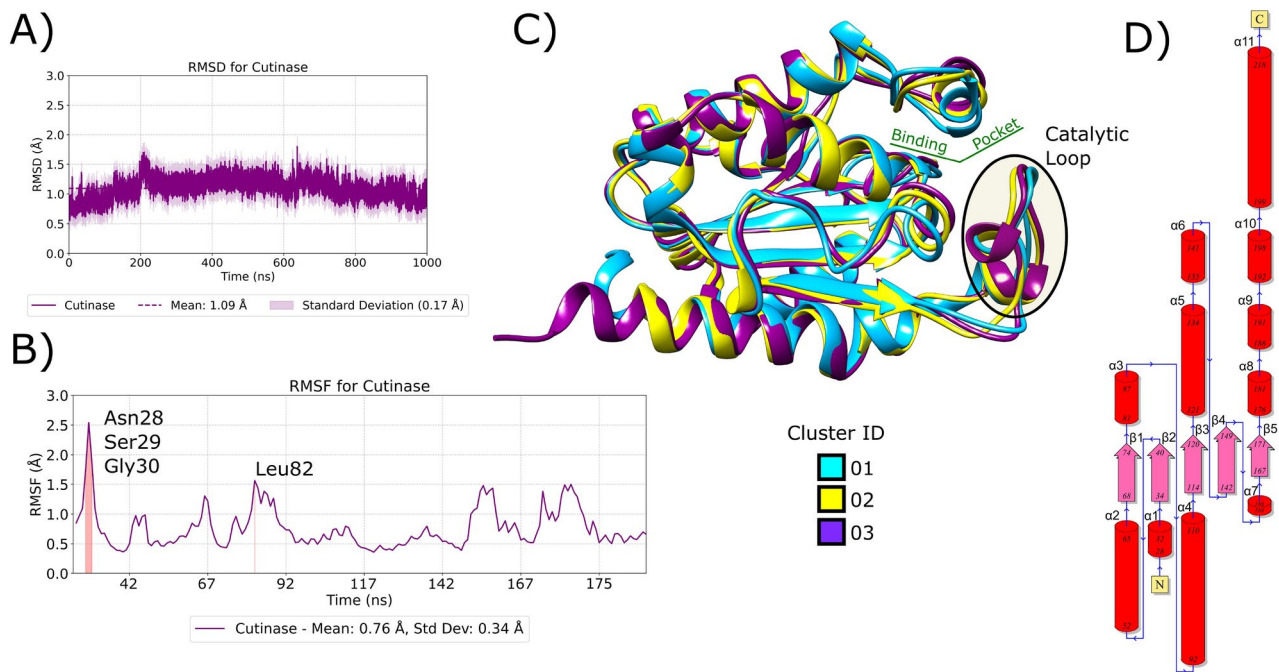


Fig. 3. Structural analysis of the *FoCut* protein in 1 μ s (1000 ns) simulation time. (A) RMSD, (B) RMSF and (C) overlapping of the centroids obtained through clustering highlighting the Catalytic Loop region based on Cluster ID and D) sequence of aminoacid described by regions.

Cluster ID	Surface (\AA^2)	Volume (\AA^3)
01	388.70	201.22
02	315.08	131.58
03	214.55	89.09

Table 2. Binding pocket grid properties by Cluster ID calculated by ProteinPlus^{91–93} using GeoMine⁹⁴.

Carrying out an analysis on the overlap of the *IsPETase* and *FoCut* proteins, we noticed that the active site region is the same for both (Fig. 2, panel D and E), which agrees with a previous contribution³⁴. Thus, we observed that the PETase using the spatial coordinates of another work on the catalytic site of the *IsPETase* enzyme³⁴, when superimposed, is in the same region in *FoCut*.

Structural analysis of the Cutinase protein from *Fusarium oxysporum*

MD simulations with a duration of 1 μ s (1000 ns) enabled us to understand the enzyme's behaviour without the presence of ligands in the active site. We observed that the enzyme highly stable throughout the simulation, with an RMSD value of 1.09 \AA (Fig. 3, panel A). A high number of hydrogen bonds between the protein residues was observed. Besides, the enzyme has two disulfide bridges between residues Cys172–Cys179 and Cys32–Cys110 as also observed in the homologous structure of Cut from *Fusarium solani*^{11,89,90}. Furthermore, the PETase enzyme presents the same disulfide bonds in the *F. solani* cutinase enzyme responsible for maintaining the stability of the active site^{1,90}.

The RMSF analysis show values below 3.0 \AA (Fig. 2, panel B), indicating that the amino acid residues exhibited minimal fluctuations during the simulation, particularly in the catalytic site region. Only fluctuations in the N- and C-terminal regions were identified, such as Asn28, Ser29, and Gly30, with values greater than 1.5 \AA . We also noted that Leu82, located in the alpha helix region at the top of the catalytic site, presented a fluctuation of 1.5 \AA . This fluctuation was influenced by the absence of ligands at the site.

We noted that during the simulation, the Cut enzyme remained predominantly at 52.6% of the simulation time, with the active site region most exposed in the clustering analysis demonstrated by volume and surface region (Table 2). It is noted that the region of the loop referring to the active site of the enzyme between residues 172–192 has movement (Fig. 3, panel C). This movement is seen with the overlap of the clusters from the highest to the lowest occupancy value (Fig. 3 and Table S1). Thus, the absence of a substrate in the active site of the enzyme causes it to remain in an open state.

Molecular Dynamics

MD simulations were performed in triplicate to evaluate the obtained data statistically. The initial analysis focused on the behavior of the ligands in the enzyme's active site. We observed that PET, PHBH, PBS, PBAT, and PCL remained in all replicates, as shown in Table 3. Therefore, only the complexes with these ligands, which remained stable across all replicates, were selected for the subsequent structural analyses.

The polymers PLA, PHB, PHBV and PES showed few strong interactions in the enzyme's active site, which resulted in the ligands leaving the active site during the simulation. The enzyme cutinase from *T. alba*¹⁹ biodegrades the PLA polymer. The cutinase of this organism, although they have the catalytic triad in common, the structure of the protein is not similar to that of the fungus *F. oxysporum*, presenting only one disulfide bond in contrast to two disulfide bonds in FoCut, which play a fundamental role in the stability of the protein and maintaining your active website. The polymer PHB and PHBH do not have data on biodegradation activity among the organisms used. In contrast to PHBH, the PHB polymer did not demonstrate strong interactions during the simulations and did not remain in the enzyme's active site. The PHBV polymer showed only a single interaction with the Thr51 residue.

In RMSD analyses (Fig. 4), considering the last minimization step as reference to all replicates, PBS and PCL exhibited considerable fluctuations in some replicates due to the instability in the structure of the ligands. The RMSD value in replicate 3 of 3.38 Å (± 0.67) for the complex with PCL and 3.69 Å (± 0.97) for PBS is due to the structural change of the polymers, as their structures are mainly involved through single bonds between the C–C atoms and C–O with very few double bonds, the sigma bonds rotate, causing the ligand to change its conformation easily quickly. During the simulation, the structures of these polymers rotate entirely, losing their stretched position initially obtained by the docking stage. This is observed by the RMSD values referring solely to these two polymers, considering only the heavy atoms (C and O), in this replicates being 4.09 Å (± 1.38) and 6.53 Å (± 1.38) for PCL and PBS respectively. This is justifiable due to the chemical structure of these polymers.

The PHBH structure remained stable across all replicates, which can be attributed to its smaller size than to the other selected polymers. We observed that the structural integrity of the PET complexes in replicates 1 and 3 was maintained throughout the 100 ns of the MD simulations. In replicate 2, the increased RMSD value was due to a conformational change in the PET structure, a behaviour that has been observed in previous studies.³⁴ Similarly, in the PBS complex, the structural change in replicate 3 was responsible for the increased RMSD value. The PBAT complex showed stability across all three replicates. This polymer contains an aromatic ring in its structure, similar to PET. This structural similarity is a crucial factor in interactions with residues at the active site, which may explain the stability of this polymer in the enzyme. The system with PBS exhibited high movement in the RMSD graph due to its structure being predominantly composed of carbon–carbon sigma bonds, which undergo rotations. These conformational changes account for the fluctuations observed in the RMSD graph. In additional RMSD analyses, we observed the behaviour of only the ligand and protein in each of the studied systems (Figures S2 and S3). This analysis revealed that the protein remained stable throughout the simulation time, regardless of the ligand, across all replicates. This demonstrates that the deviations in the RMSD of the complexes are directly attributable to the ligands. Furthermore, an additional MD simulation analysis of only the protein further confirms the stability of this enzyme during the simulation.

All systems demonstrated that the enzyme remained stable, with fluctuations not exceeding 3.0 Å (Fig. 5). This is consistent with the RMSD analysis data, where we showed that the instability of a system is directly related to the ligand. The RMSF data indicate a similar fluctuation profile across all six best systems and across all replicates. A slight fluctuation was observed in the system with PCL in repetition 2, resulting in more significant fluctuations than the others. This fluctuation is attributed to a structural change in the ligand in this replicate, leading to weaker interactions and consequently greater fluctuation. None of the systems showed significant fluctuation for the catalytic triad residues Ser121, His189, and Asp176.

We applied the clustering methodology to each replicate individually, as well as to the entire set, to evaluate the ligand conformation in each replicate. We determined how the structure was maintained by identifying the most populous cluster (Table S2). The PET analysis demonstrated that in replicates 1 and 3 (with simulation time fractions of 43.5% and 50.5%, respectively). The PET presented a similar structure and in replicate 2 (with

FoCut complex	Replicates			Permanency (%)
	01	02	03	
PET	*	*	*	100
PLA	–	–	–	0
PHB	–	–	–	0
PHBH	*	*	*	100
PHBV	–	–	–	0
PBS	*	*	*	100
PBAT	*	*	*	100
PCL	*	*	*	100
PES	–	–	–	0

Table 3. Permanency of polymers in the catalytic site of the FoCut enzyme in each of the complexes and the percentage of polymers remaining in the three replicates. (*) represent the 100% permanency of the polymer in active site during all simulation time, (–) the polymer left the active site during the simulation time.

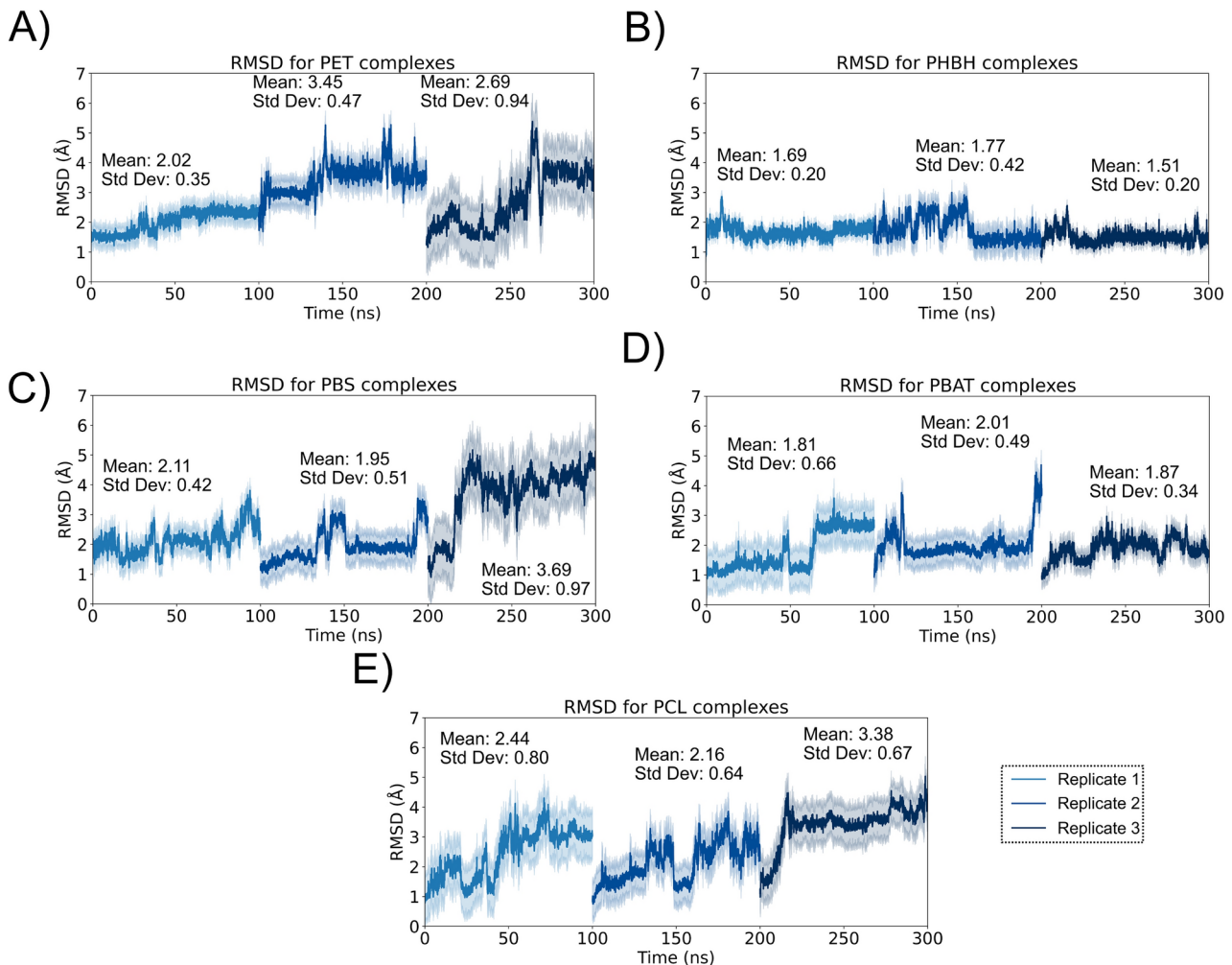


Fig. 4. Root mean square deviation (RMSD) for the backbone atoms (C, O, Ca, and N) plots obtained from FoCut complexes for all replicates. (A) PET, (B) PHBH, (C) PBS, (D) PBAT and (E) PCL complexes.

46%) the single bonds between carbons rotated as demonstrated in another Molecular Dynamics study with PET complexed to PETase³⁴. Considering the 3 replicates together in total, the structure obtained is similar to that obtained in replicates 1 and 3 with a time fraction of 68.9% (Figure S5). For complexes with PBAT, the replicates did not show much similarity, even with the similar RMSD between the replicates. Each structure did not remain stable in the simulation with values below 40% of the simulation time fraction, with the total pose being 36.9%. The aromatic ring present in both PBAT and PET carries out pi interactions with protein residues in the catalytic site.

The interactions between the ligands with the amino acids of the catalytic site of the FoCut enzyme were computed through fingerprint analysis with the ProLif program, demonstrating that the main interactions that are carried out for the complex with PET in the three replicates are Leu82, Ala86, Leu183, Val185, Leu190. The first replicate presented more interactions with an occurrence greater than 0.5 with the residues of the site, which directly explains the stable RMSD during the simulation time.

Moreover, residues Tyr120 and His189 perform pi interactions with the aromatic rings of both ligands (Fig. 6, panel B and D). For complexes with PBAT, the main residues that interact in the three replicates are Tyr120, Val185, Leu190. The same situation is present in PET, the most stable system in RMSD, which is consequently the one that performs the most fingerprint interactions in complexes with PBAT. We also highlight that both complexes are formed mainly through hydrophobic, van der Waals and pi interactions. Both interact with the critical residue His189, corresponding to a catalytic residue. Furthermore, the catalytic Serine in Cutinase from *T. fusca* is involved in the PBAT degradation mechanism²².

Complexes with PHBH carry out interactions with residues Ser43, Leu82, Gln122, Leu183, Val185, Leu190 in all replicate (Fig. 7). However, the catalytic residue His189 in two replicates has an occurrence value greater than 0.5, in replicate 2 this value is the opposite (less than 0.5), but in the total calculation, this contribution appears as a strong interaction as well as Glu45 and Tyr120. Furthermore, in replicate 1, another catalytic residue interacts with the ligand, Ser121. The main interactions forming these complexes with PHBH are van der Waals and hydrophobic, with only a single hydrogen bond with the Ser43 residue.

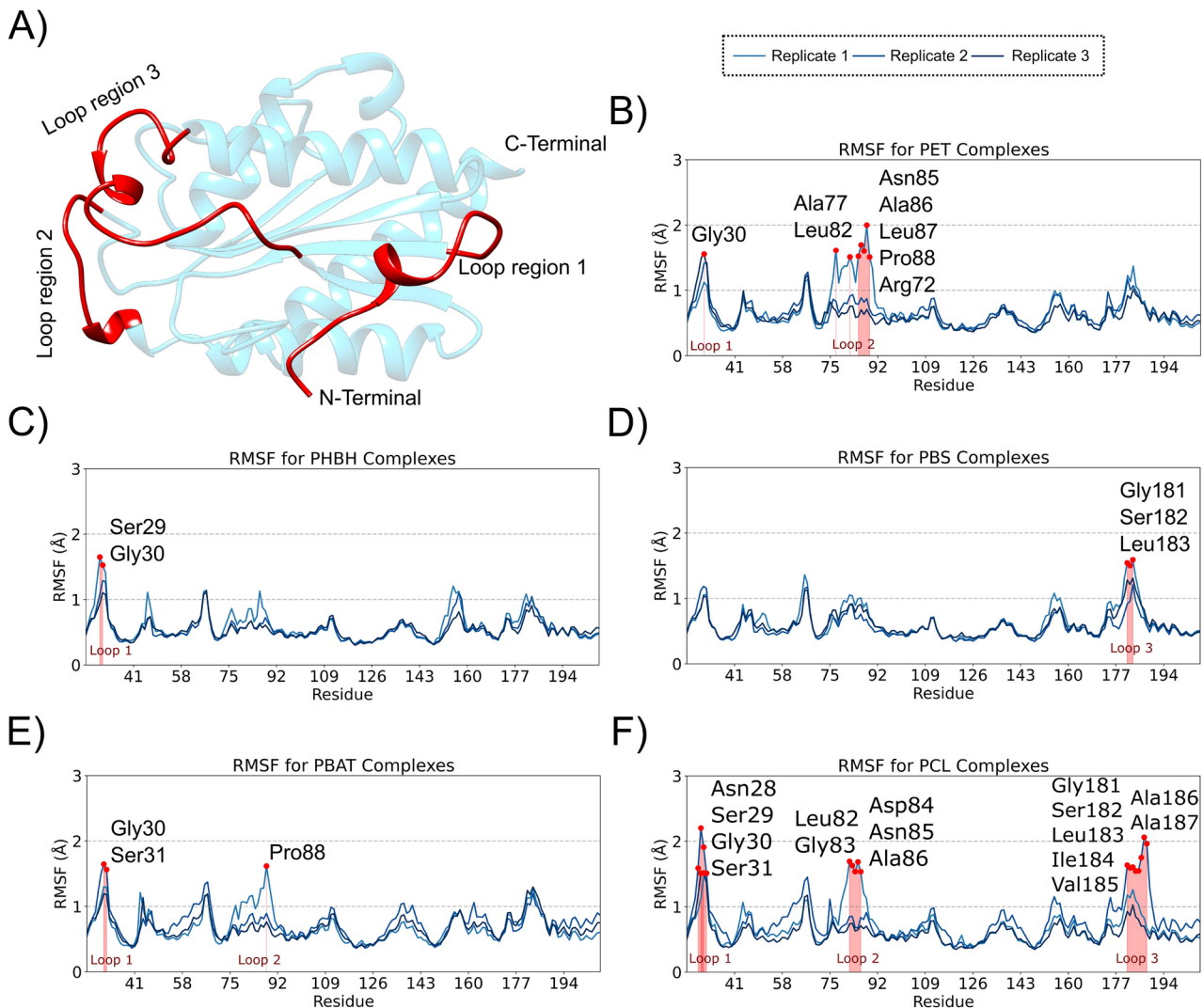


Fig. 5. Root mean square fluctuation (RMSF) plots obtained from *FoCut* complexes for each Replicate and (A) tridimensional structure of *FoCut* highlighting the loop regions, N-Terminal and C-Terminal. (B) PET, (C) PHBH, (D) PBS, (E) PBAT and (F) PCL complexes.

Complexes with PBS are mainly formed by hydrophobic van der Waals interactions (Fig. 7). However, the polymer also performs an anionic interaction (Arg55) and two hydrogen bonds (Ser43, Arg55), with the Arg55 residue only in replicate 1. The residues Ser43, Leu82, Tyr120, Ser121, Gln122, Leu183, Val185, Leu190 perform interactions of van der Waals and hydrophobic in the 3 replicates. Furthermore, residue His189 appears in two replicates and is also a essential interaction residue. In this way, we observed that PBS is one of the best ligands due to its high number of interactions and the high occurrence value of these interactions that the ligand performs with residues of the catalytic site.

PCL interacts with residues Ser43, Leu82, Tyr120, Val185, Leu190 in the three replicates to form PCL-*FoCut* complexes (Figure S5, panel C). The interactions involved in forming of this complex are predominantly van der Waals and hydrophobic, but the ligand performs hydrogen interactions with residues Ser43 and Leu82 in replicate 2. This demonstrates that during this replicate, the ligand was closer to these residues than in the other replicates, which justifies its having the lowest RMSD value. The absence of strong interactions in replicate 3 causes the ligand to carry out more movements at the site than a system with more entries, which justifies the high RMSD value of this replicate. PCL complex in *MrCut* can be biodegraded by the enzyme¹². Our study identified the affinity of the ligand to interact with residues from the *FoCut* enzyme site of another organism. This demonstrates that Cutinase enzymes can function as biocatalysts in polymer degradation reactions regardless of the organism. This information provides insights into the critical amino acid residues of the catalytic site that are involved in forming the enzyme–substrate complex.

Through the interactions that polymers carry out in the active site of the enzyme, the key residues Ser43, Val185 and Leu190 are in the active site and contribute for the formation of all polymer-*FoCut* complexes studied. Where the Ser43 residue, as well as Gln122, is present in the region of the oxyanion hole⁹⁵.

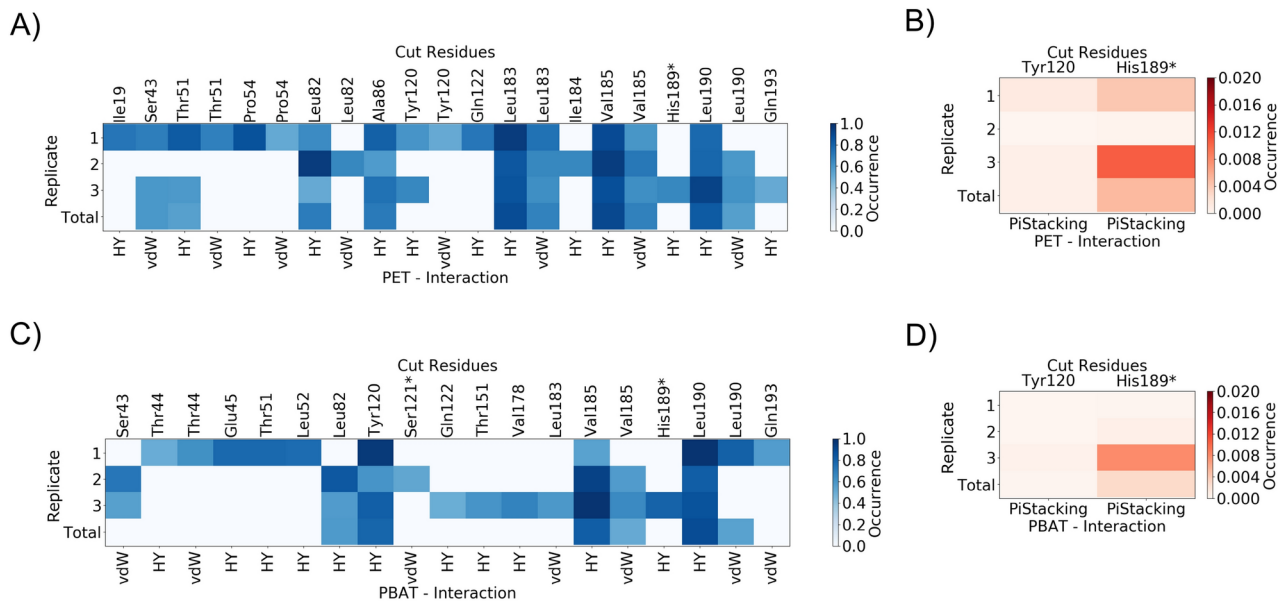


Fig. 6. Interaction fingerprints (IFP) of FoCut complexes, including interaction information—and the occurrence of each interaction—as hydrophobic (HY), van der Waals (vdW) and PiStacking character interactions for A–B) PET and PBAT C–D) complexes, respectively.

In the clustering analysis (Figure S6), PHBH presented similar structures in replicates 1 and 3 and in the total structure (considering all 3 replicates together). This demonstrates that the ligand remained predominantly in a similar conformation in the enzyme's active site during all simulations (73.5%). The same is observed in the PBS structures in replicates 2 and total. This structure of the second replicate appears stable structure during 70.1% of the total simulation time of the three replicates together. For the system with PCL, the majority structure of replicate 3 is identical to the total structure of the replicates, however, replicates 1 and 2 are completely different, showing that the ligand can present these other two conformations due to its high number of sigma bonds that rotate during simulation. This conformational change demonstrates that the conformation of replicate 2 (with 54.3% presence during the simulation time) performs strong interactions at the site, which demonstrates that it is a critical conformation that performs interactions with the catalytic residue Ser121 in addition to interaction with Leu190, which is a residue key in protein stabilization through the alpha helix⁹⁵.

The analysis of the distance between the polymers, considering the representative pose of the clustering carried out with the three simulations together (Total Cluster, Figures S5 and S6) and the catalytic residues demonstrated that in some systems the catalytic Serine is considerably close to the carbon of the ester group in the polymer structure, enabling nucleophilic attack to cleave the polymer structure. The PBS polymers presented the smallest distance from the carbon of the ester group and Ser121. The PET polymer during the simulation approached Ser121, moving from an initial distance of 6.4 to 4.1 Å (Figure S1 and Fig. 8). PBAT presented a distance of 4.2 Å and PCL with 4.8 Å. The rotation of the C–C single bonds caused the PHBH polymer to lose interaction with residue Ser121, however, in replicate 1 this interaction is maintained firmly during the simulation. This shows that no matter how much the conformational change occurred in the total replicate, Ser121 aims to interact with this carbon of the Ester group of the polymer so that the nucleophilic attack occurs. This information serves as a starting point for elucidating the reaction mechanism of polymers biodegraded by FoCut and also of other Cutinase from organisms.

Polymers complexes binding affinities

The binding free energy data demonstrate that PET is the polymer with the highest affinity for the Cutinase enzyme (Table 4). Experimental methods, such as microscopy, have shown and confirmed the ability of the fungus *Fusarium oxysporum* to biodegrade PET-type polymers through the Cutinase enzyme⁵⁴. Among the nine polymers studied, five exhibit affinity for the Cutinase enzyme, with PET having the most excellent affinity at $-34.26 (\pm 5.51)$ kcal/mol. In addition to PET, the polymers PHBH, PBS, PBAT, and PCL also showed high binding affinity with the FoCut enzyme, with values of $-18.44 (\pm 4.41)$, $-29.71 (\pm 5.90)$, $-22.78 (\pm 5.36)$, and $-22.26 (\pm 6.56)$ kcal/mol, respectively. In 2021, it was discovered that Cutinase from *M. roreri* can biodegrade PES, PCL and PET polymers with degradation percentages of 59%, 43% and 31%, respectively, after 21 days¹². This demonstrates that *MrCut1* can biodegrade polymers other than PET, with a greater affinity for the PES polymer. In the case of FoCut, the PES polymer showed little affinity and did not remain bound for the entire simulation, dissociating at approximately 80 ns. Therefore, the binding free energy value of $-13.57 (\pm 8.63)$ kcal/mol suggests that further studies are needed to explore the potential of FoCut to degrade this polymer. However, PCL and PET polymers showed a binding affinity with the FoCut enzyme. *KrCut* has demonstrated the ability to biodegrade PCL polymers and the synthetic polyester poly(1,3-propylene adipate)¹⁸. As with *KrCut*, FoCut

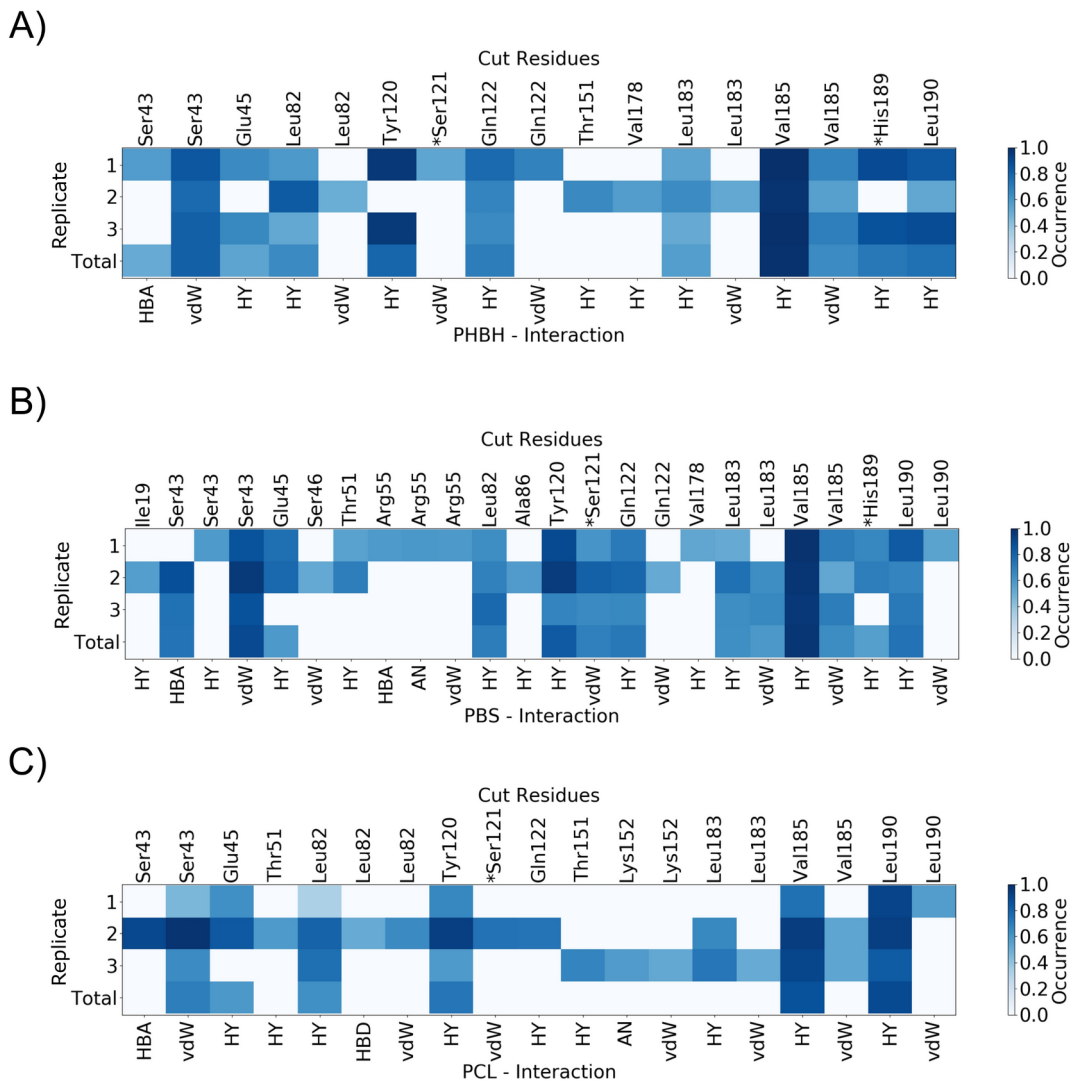


Fig. 7. Interaction fingerprints (IFP) of FoCut complexes, including interaction information—and the occurrence of each interaction—as hydrophobic (HY), van der Waals (vdW) and Hydrogen bond donor (HBD), Hydrogen bond Acceptor (HBA) and Anionic (AN) character interactions for A) PHBH, B) PBS and C) PCL complexes, respectively.

also showed binding affinity with the PCL polymer, demonstrating that even though they are from different organisms, the *MrCut1* and *KrCut* enzymes have the same affinity for PCL.

The system with PET exhibited the most favorable residues, which is consistent with its highest affinity value. The smaller the ΔG value and the greater the number of interactions, the more favourable residues are involved. The main residues contributing to the ΔG_{total} value in the three replicates for PET are Leu82, Ala86, Leu183, Val185, and Leu190. In the complexes with PHBH, the residues that consistently contributed across the three replicates are Ser43, Leu82, Gln122, Leu183, and Leu185 (Figure S7). In the complex with PBS, most of the central residues contribute to the three replicates being Gly42, Ser43, Leu82, Tyr120, *Ser121, Gln122, Leu183, Val185 and Leu190. In the system with PBAT, only three main residues contribute to all replicates, Leu82, Val185, and Leu190. In the last system, the complexes with PCL, only two residues appear, contributing to all replicates Val185 and Leu190.

The amino acid residues Val185 and Leu190 were favorable in all replicates across all five systems (Figure S7), demonstrating their key role in complex formation through van der Waals and hydrogen interactions. These residues are part of the catalytic loop region (Fig. 3, panel C), confirming its importance in maintaining the polymer in the active site. These common residues in all systems across the three replicates indicate that all polymers remained in the same region of the enzyme's active site. Additionally, the Leu82 residue, located in another loop region, is highlighted as crucial for maintaining the stability of the polymer complexes, as this region exhibits high fluctuation in the absence of polymers (Fig. 3). Furthermore, the Ser121 catalytic residues were favorable for at least one replicate of the complexes performing van der Waals interaction. As this movement only happens in these replicates, through fingerprint analysis we were able to visualize that some interactions carried out in these replicates are not carried out in the others due to the unique rotational movement of the single bonds in the

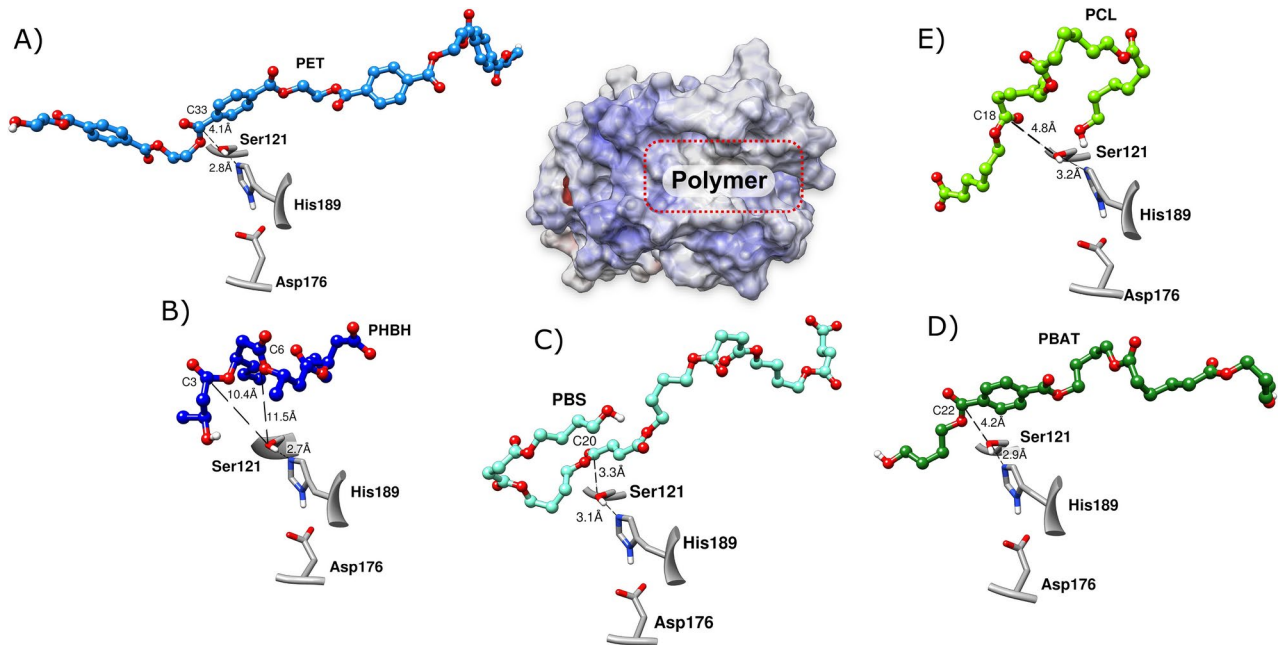


Fig. 8. Total cluster centroid of (A) PET, (B) PHBH, (C) PBS, (D) PBAT and (E) PCL polymers in the catalytic site in relation to the distance from the *FoCut* catalytic triad.

	FoCut complex									
Energy	PET	PLA	PHB	PHBH	PHBV	PBS	PBAT	PCL	PES	
vdW	-50.06 (±6.06)	-7.22 (±5.78)	-13.16 (±8.92)	-26.41 (±3.03)	-10.48 (±9.24)	-40.27 (±5.78)	-33.17 (±5.43)	-29.91 (±6.73)	-17.62 (±11.44)	
EEL	-12.09 (±8.92)	-70.64 (±44.52)	-75.49 (±29.82)	-80.20 (±8.05)	-66.95 (±36.95)	-132.36 (±45.72)	-12.04 (±7.69)	-115.63 (±40.49)	-115.49 (±50.11)	
ΔG_{gas}	-62.15 (±12.31)	-77.85 (±45.32)	-88.65 (±33.89)	-106.61 (±9.30)	-77.43 (±41.79)	-172.63 (±46.66)	-45.20 (±1070)	-145.55 (±41.99)	-132.78 (±54.31)	
EGB	36.06 (±9.02)	74.09 (±43.10)	11.65 (±30.90)	92.71 (±7.28)	72.33 (±38.03)	150.29 (±43.56)	28.09 (±7.19)	128.79 (±39.13)	123.00 (±49.14)	
ESURF	-8.18 (±0.98)	-1.43 (±1.03)	-2.48 (±1.54)	-4.54 (±0.45)	-1.95 (±1.62)	-7.36 (±0.98)	-5.67 (±0.98)	-5.50 (±1.18)	-3.46 (±1.94)	
ΔG_{solv}	27.89 (±8.36)	72.66 (±42.67)	80.93 (±30.07)	88.17 (±7.10)	-70.38 (±36.97)	142.91 (±43.03)	-22.42 (±6.57)	-123.29 (±38.57)	-119.54 (±48.03)	
ΔG_{total}	-34.26 (±5.51)	-5.19 (±5.04)	-8.72 (±6.25)	-18.44 (±4.41)	-7.05 (±6.54)	-29.71 (±5.90)	-22.78 (±5.36)	-22.26 (±6.56)	-13.57 (±8.63)	

Table 4. Binding free energy values (from MM/GBSA method) for the *FoCut* complexes.

polymer structure during these simulations. This character is not shown in the other replicates, which suggests that it is unique and particular to these replicates in isolation, as in replicate 2 of the complex with PBS this residue contributes favorably.

Conclusion

Our phylogenetic analysis provided important insights into the biological similarity of enzymes that biodegrade polymers in different types of organisms. It demonstrated that although *F. oxysporum* cutinase is not closely related to *KrCut* and *MrCut*, they all can biodegrade polymers. Thus, these discoveries show that even though bacteria or fungi produce them, these enzymes have this biological similarity of biodegrading polymers. Therefore, our findings provide the critical information that *FoCut* is like Cutinase from several organisms such as *Aspergillus oryzae*, *Moniliophthora roreri*, *Paraphoma* sp., *Humicola insolens*, *Saccharomonospora viridis*, *Thermobifida fusca*, *Fusarium solani*. Furthermore, an overlap analysis demonstrate that both *FoCut* and *IsPETase* enzymes have the catalytic triad in the same region, which also justifies the similarity of the region in which PET was inserted through Molecular Docking, being similar to the *IsPETase* enzyme site region as already demonstrated in the literature. Furthermore, our data demonstrate that the polymers PET, PHBH, PBS, PBAT, and PCL can bind into Cutinase enzyme from *Fusarium oxysporum*, demonstrating the possibility of biodegradation activity of these new polymers in addition to PET (-34.26 ± 5.51), which has already been reported in the literature as a polymer degraded by this enzyme, with binding free energy values equal to $-18.44 (\pm 4.41)$, -29.71

(± 5.90), -22.78 (± 5.36), and -22.26 (± 6.56) kcal/mol, respectively. We therefore demonstrated, through computational simulations, the stability through the intermolecular interactions of these polymers in the active site, highlighting the importance of key residues such as Val185 and Leu190 that are involved in an opening loop—also called catalytic loop—responsible for causing the polymers remain in the active site. We highlight the Ser43 and Gln122 exclusion as one of the key residues important to coordinate the ester group region and keep the ligands close to the catalytic triad through the oxyanion hole. Furthermore, we highlight the polymer binding mode through predominantly vdW and hydrophobic interactions to form the polymer–FoCut complex. The cleavage mechanism of these polymers through the ester group, by the nucleophilic attack of the catalytic Serine, in their structures demonstrates the similarity between cutinases and PETases enzymes. Thus, our work provides a new perspective for using Cut enzymes, especially FoCut, as biocatalysts for polymer degradation reactions, providing insights into the possibility of enzymatic improvement to increase their enzymatic activity.

Data availability

The datasets used and/or analysed during the current study available from the corresponding author on reasonable request.

Received: 30 June 2024; Accepted: 26 December 2024

Published online: 22 January 2025

References

- Austin, H. P. et al. Characterization and engineering of a plastic-degrading aromatic polyesterase. *Proc. Natl. Acad. Sci. USA* **115**, E4350–E4357 (2018).
- Han, X. et al. Structural insight into catalytic mechanism of PET hydrolase. *Nat. Commun.* **8**, 2106 (2017).
- Joo, S. et al. Structural insight into molecular mechanism of poly(ethylene terephthalate) degradation. *Nat. Commun.* **9**, 382 (2018).
- Rhodes, C. J. Plastic pollution and potential solutions. *Sci. Prog.* **101**, 207–260 (2018).
- Kankanige, D. & Babel, S. Smaller-sized micro-plastics (MPs) contamination in single-use PET-bottled water in Thailand. *Sci. Total Environ.* **717**, 137232 (2020).
- Samir, A., Ashour, F. H., Hakim, A. A. A. & Bassyouni, M. Recent advances in biodegradable polymers for sustainable applications. *Npj Mater. Degrad.* **6**, 68 (2022).
- Roman, L., Schuyler, Q., Wilcox, C. & Hardesty, B. D. Plastic pollution is killing marine megafauna, but how do we prioritize policies to reduce mortality?. *Conserv. Lett.* **14**, 12871 (2021).
- Benavides Fernández, C. D., Guzmán Castillo, M. P., Quijano Pérez, S. A. & Carvajal Rodríguez, L. V. Microbial degradation of polyethylene terephthalate: A systematic review. *SN Appl. Sci.* **4**, 263 (2022).
- Kanwal, A., Zhang, M., Sharaf, F. & Li, C. Polymer pollution and its solutions with special emphasis on Poly (butylene adipate terephthalate (PBAT)). *Polym. Bull.* **79**, 9303–9330 (2022).
- Hellesnes, K. N., Vijayaraj, S., Fojan, P., Petersen, E. & Courtade, G. Biochemical Characterization and NMR Study of a PET-hydrolyzing cutinase from *Fusarium solani pisi*. *Biochemistry* **62**, 1369–1375 (2023).
- Dimarogona, M. et al. Structural and functional studies of a *Fusarium oxysporum* cutinase with polyethylene terephthalate modification potential. *Biochim. Biophys. Acta BBA General Subjects* **1850**, 2308–2317 (2015).
- Vázquez-Alcántara, L., Oliart-Ros, R. M., García-Bórquez, A. & Peña-Montes, C. Expression of a cutinase of *Moniliophthora roreri* with polyester and PET-plastic residues degradation activity. *Microbiol. Spectr.* **9**(3), e00976-e1021 (2021).
- Numoto, N. et al. Structural dynamics of the PET-degrading cutinase-like enzyme from *Saccharomonospora viridis* AHK190 in substrate-bound states elucidates the Ca^{2+} –driven catalytic cycle. *Biochemistry* **57**, 5289–5300 (2018).
- Ribitsch, D. et al. Characterization of a new cutinase from *Thermobifida alba* for PET-surface hydrolysis. *Biocatal Biotransform.* **30**, 2–9 (2012).
- Zhang, Z. et al. Depolymerization of post-consumer PET bottles with engineered cutinase 1 from *Thermobifida cellulosilytica*. *Green Chem.* **24**, 5998–6007 (2022).
- Furukawa, M., Kawakami, N., Tomizawa, A. & Miyamoto, K. Efficient degradation of poly(ethylene terephthalate) with thermobifida fusca cutinase exhibiting improved catalytic activity generated using mutagenesis and additive-based approaches. *Sci. Rep.* **9**, 16038 (2019).
- Aristizábal-Lanza, L., Mankar, S. V., Tullberg, C., Zhang, B. & Linares-Pastén, J. A. Comparison of the enzymatic depolymerization of polyethylene terephthalate and AkestaTM using *Humicola insolens* cutinase. *Front. Chem. Eng.* **4**, 1048744 (2022).
- Abokitse, K. et al. A novel actinobacterial cutinase containing a noncatalytic polymer-binding domain. *Appl. Environ. Microbiol.* **88**, e015221. <https://doi.org/10.1128/AEM.01522-21> (2022).
- Kitadokoro, K. et al. Structural insights into the unique polylactate-degrading mechanism of *Thermobifida alba* cutinase. *FEBS J.* **286**, 2087–2098 (2019).
- Gamerith, C. et al. Enzymatic degradation of aromatic and aliphatic polyesters by *P. pastoris* expressed cutinase 1 from *Thermobifida cellulosilytica*. *Front. Microbiol.* **8**, (2017).
- Hu, X. et al. Enzymatic degradation of poly(butylene succinate) by cutinase cloned from *Fusarium solani*. *Polym. Degrad. Stab.* **134**, 211–219 (2016).
- Yang, Y. et al. Complete bio-degradation of poly(butylene adipate-co-terephthalate) via engineered cutinases. *Nat. Commun.* **14**, 1645 (2023).
- Lin, W., Zhao, Y., Su, T. & Wang, Z. Enzymatic hydrolysis of poly(butylene adipate-co-terephthalate) by *Fusarium solani* cutinase. *Polym. Degrad. Stab.* **211**, 110335 (2023).
- Abdel-Azeem, A. M., Abdel-Azeem, M. A., Darwish, A. G., Nafady, N. A. & Ibrahim, N. A. Fusarium: Biodiversity, ecological significances, and industrial applications. 201–261 (Springer Nature, 2019).
- Steinberg, C. et al. Adaptation of *Fusarium oxysporum* and *Fusarium dimerum* to the specific aquatic environment provided by the water systems of hospitals. *Water Res.* **76**, 53–65 (2015).
- Barata, L. M. et al. Secondary metabolic profile as a tool for distinction and characterization of cultivars of black pepper (*Piper nigrum* L.) cultivated in Pará State. *Brazil. Int. J. Mol. Sci.* **22**, 890 (2021).
- Paracampo, N. E., Abreu, L. F. de Lemos, O. F. & Both, J. P. Quality Of black pepper produced in northeastern Pará. *Rev. De Agric. Neotrop.* **9**(3), e7020 (2022).
- Bubici, G., Kaushal, M., Prigigallo, M. I., Gómez-Lama Cabanás, C. & Mercado-Blanco, J. Biological control agents against fusarium wilt of Banana. *Front. Microbiol.* **10**, (2019).
- McGovern, R. J. Management of tomato diseases caused by *Fusarium oxysporum*. *Crop Protection* **73**, 78–92 (2015).

30. de Oliveira, M. V., Fernandes, G. M., da Costa, K. S., Vakal, S. & Lima, A. H. Virtual screening of natural products against 5-enolpyruvylshikimate-3-phosphate synthase using the *Anagreen herbicide*-like natural compound library. *RSC Advances.* **12**(29), 18834–18847 (2022).
31. De Oliveira, M. D., Araújo, J. de O., Galúcio, J. M. P., Santana, K. & Lima, A. H. Targeting shikimate pathway: In silico analysis of phosphoenolpyruvate derivatives as inhibitors of EPSP synthase and DAHP synthase. *J. Mol. Graph Model* **101**, 107735 (2020).
32. De Souza, E. M. de C. et al. Molecular characterization and in silico evaluation of surfactins produced by endophytic bacteria from *Phanera splendens*. *Front. Chem.* **11**, 1240704 (2023).
33. de Oliveira, M. V., Almeida, L., da Rocha, J., Wanzeller, A. L. & Lima, A. A combined approach for predicting binding affinity of Zika Virus NS2B-NS3 protease inhibitors using semi-empirical methods and molecular docking algorithms. *J. Braz. Chem. Soc.* <https://doi.org/10.21577/0103-5053.20230130> (2024).
34. Costa, C. H. S. et al. Assessment of the PETase conformational changes induced by poly(ethylene terephthalate) binding. *Proteins Struct. Funct. Bioinform.* **89**, 1340–1352 (2021).
35. Araújo, O. J. et al. Structural, energetic and lipophilic analysis of SARS-CoV-2 non-structural protein 9 (NSP9). *Sci. Rep.* **11**, 23003 (2021).
36. Tamura, K., Stecher, G. & Kumar, S. MEGA11: Molecular evolutionary genetics analysis version 11. *Mol. Biol. Evol.* **38**, 3022–3027 (2021).
37. Avilan, L. et al. Concentration-dependent inhibition of mesophilic PETases on poly (ethylene terephthalate) can be eliminated by enzyme engineering. *ChemSusChem.* **16**(8), e202202277 (2023).
38. Longhi, S., Czjzek, M., Lamzin, V., Nicolas, A. & Cambillau, C. Atomic resolution (1.0 Å) crystal structure of *Fusarium solani* cutinase: stereochemical analysis. *J. Mol. Biol.* **268**, 779–799 (1997).
39. Martinez, C., De Geus, P., Lauwereys, M., MatthysSENS, G. & Cambillau, C. *Fusarium solani* cutinase is a lipolytic enzyme with a catalytic serine accessible to solvent. *Nature* **356**, 615–618 (1992).
40. Kold, D. et al. Thermodynamic and structural investigation of the specific SDS binding of *humicola insolens* cutinase. *Protein Science* **23**, 1023–1035 (2014).
41. Nyon, M. P. et al. Catalysis by *glomerella cingulata* cutinase requires conformational cycling between the active and inactive states of its catalytic triad. *J. Mol. Biol.* **385**, 226–235 (2009).
42. Liu, Z. et al. Structural and functional studies of *Aspergillus oryzae* cutinase: Enhanced thermostability and hydrolytic activity of synthetic ester and polyester degradation. *J. Am. Chem. Soc.* **131**, 15711–15716 (2009).
43. Duan, X. et al. High-level expression and characterization of a novel cutinase from *Malbranchea cinnamomea* suitable for butyl butyrate production. *Biotechnol. Biofuels* **10**, 223 (2017).
44. Roussel, A. et al. A cutinase from *trichoderma reesei* with a lid-covered active site and kinetic properties of true lipases. *J. Mol. Biol.* **426**, 3757–3772 (2014).
45. Miyakawa, T. et al. Structural basis for the Ca²⁺-enhanced thermostability and activity of PET-degrading cutinase-like enzyme from *Saccharomonospora viridis* AHK190. *Appl. Microbiol. Biotechnol.* **99**, 4297–4307 (2015).
46. Erickson, E. et al. Sourcing thermotolerant poly(ethylene terephthalate) hydrolase scaffolds from natural diversity. *Nat. Commun.* **13**, 7850 (2022).
47. Ribitsch, D. et al. Small cause, large effect: Structural characterization of cutinases from *Thermobifida cellulosilytica*. *Biotechnol. Bioeng.* **114**, 2481–2488 (2017).
48. Kitadokoro, K. et al. Crystal structure of cutinase Est119 from *Thermobifida alba* AHK119 that can degrade modified polyethylene terephthalate at 1.76 Å resolution. *Polym. Degrad. Stab.* **97**, 771–775 (2012).
49. Berman, H. M. et al. The protein data bank. *Nucl. Acids Res.* <https://doi.org/10.1093/nar/28.1.235> (2000).
50. ChemAxon. ChemAxon—Software Solutions and Services for Chemistry and Biology. *MarvinSketch*, Version 16.10.31 Preprint at (2016).
51. Hanwell, M. D. et al. Avogadro: An advanced semantic chemical editor, visualization, and analysis platform. *J. Cheminform.* <https://doi.org/10.1186/1758-2946-4-17> (2012).
52. Frisch, M. J. ; et. al. Nathan, A. J. & Scobel, A. Gaussian 09. *Gaussian, Inc. Wallingford CT* 2–3 Preprint at 111 (2009).
53. Roothaan, C. C. J. New developments in molecular orbital theory. *Rev. Mod. Phys.* **23**, 69–89 (1951).
54. Cognigni, F. et al. Exploring the infiltrative and degradative ability of *Fusarium oxysporum* on polyethylene terephthalate (PET) using correlative microscopy and deep learning. *Sci. Rep.* **13**, 22987 (2023).
55. Santos-Benito, F. et al. Screening enzymes that can depolymerize commercial biodegradable polymers: Heterologous expression of *fusarium solani* cutinase in *Escherichia coli*. *Microorganisms* **11**, 328 (2023).
56. Liang, X. & Zou, H. Biotechnological application of cutinase: A powerful tool in synthetic biology. *SynBio* **1**, 54–64 (2022).
57. Huang, Q., Kimura, S. & Iwata, T. Thermal embedding of *Humicola insolens* cutinase: A strategy for improving polyester biodegradation in seawater. *Biomacromolecules* **24**, 5836–5846 (2023).
58. Suzuki, M., Tachibana, Y. & Kasuya, K. Biodegradability of poly(3-hydroxyalkanoate) and poly(ϵ -caprolactone) via biological carbon cycles in marine environments. *Polym. J.* **53**, 47–66 (2021).
59. Murphy, C. A., Cameron, J. A., Huang, S. J. & Vinopal, R. T. Fusarium polycaprolactone depolymerase is cutinase. *Appl. Environ. Microbiol.* **62**, 456–460 (1996).
60. Thomsen, R. & Christensen, M. H. MolDock: A new technique for high-accuracy molecular docking. *J. Med. Chem.* **49**, 3315–3321 (2006).
61. Jones, G., Willett, P., Glen, R. C., Leach, A. R. & Taylor, R. Development and validation of a genetic algorithm for flexible docking 1 Edited by F E. Cohen. *J. Mol. Biol.* **267**, 727–748 (1997).
62. Jurrus, E. et al. Improvements to the <scp>APBS</scp> biomolecular solvation software suite. *Protein Sci.* **27**, 112–128 (2018).
63. Jo, S., Kim, T., Iyer, V. G. & Im, W. CHARMM-GUI: A web-based graphical user interface for CHARMM. *J. Comput. Chem.* **29**, 1859–1865 (2008).
64. Brooks, B. R. et al. CHARMM: The biomolecular simulation program. *J. Comput. Chem.* **30**, 1545–1614 (2009).
65. Lee, J. et al. CHARMM-GUI input generator for NAMD, GROMACS, AMBER, OpenMM, and CHARMM/OpenMM simulations using the CHARMM36 additive force field. *J. Chem. Theory Comput.* **12**, 405–413 (2016).
66. Jorgensen, W. L., Chandrasekhar, J., Madura, J. D., Impey, R. W. & Klein, M. L. Comparison of simple potential functions for simulating liquid water. *J. Chem. Phys.* <https://doi.org/10.1063/1.445869> (1983).
67. Case, D. A. et al. Amber 20. (2020).
68. Srinivasan, J., Cheatham, T. E., Cieplak, P., Kollman, P. A. & Case, D. A. Continuum solvent studies of the stability of DNA, RNA, and phosphoramidate–DNA helices. *J. Am. Chem. Soc.* **120**, 9401–9409 (1998).
69. Miller, B. R. III. et al. MMPSA. py: An efficient program for end-state free energy calculations. *J. Chem. Theory Comput.* **8**(9), 3314–3321 (2012).
70. Genheden, S. & Ryde, U. The MM/PBSA and MM/GBSA methods to estimate ligand-binding affinities. *Expert Opin. Drug Discov.* **10**, 449–461 (2015).
71. Wang, L., Pang, X., Li, Y., Zhang, Z. & Tan, W. RADER: A RApid DEcoy retriever to facilitate decoy based assessment of virtual screening. *Bioinformatics* **33**, 1235–1237 (2017).
72. Wang, E. et al. End-point binding free energy calculation with MM/PBSA and MM/GBSA: Strategies and applications in drug design. *Chem. Rev.* **119**, 9478–9508 (2019).

73. Koitabashi, M. et al. Biodegradable plastic-degrading activity of various species of <i>P</i><i>araphoma</i>. *J Oleo Sci* **65**, 621–627 (2016).
74. Dsouza, G. C. et al. Fungal biodegradation of low-density polyethylene using consortium of *Aspergillus* species under controlled conditions. *Heliyon* **7**, e7008 (2021).
75. Choi, J. et al. Recent advances in microbial and enzymatic engineering for the biodegradation of micro- and nanoplastics. *RSC Adv.* **14**, 9943–9966 (2024).
76. Huang, Q.-S. et al. Accelerated biodegradation of polyethylene terephthalate by *Thermobifida fusca* cutinase mediated by *Stenotrophomonas pavani*. *Sci. Total Environ.* **808**, 152107 (2022).
77. Scattolini Rimada, A. C., Hernández Rodríguez, L. I. & González Idiarte, H. Identification of *Fusarium oxysporum* causing sweet potato rot (*Ipomoea batatas* L & Lamb) in Uruguay. *Agrociencia* **24**, e124 (2020).
78. Rodríguez-Grimaldo, J. E., M. González, G. & M. Montoya, A. *Fusarium: Un fitopatógeno Que Amenaza La Salud Humana. Revista Ciencia UANL* **25**, 37–43 (2023).
79. Cighir, A. et al. *Fusarium* spp. in Human Disease: Exploring the Boundaries between Commensalism and Pathogenesis. *Life* **13**, 1440 (2023).
80. Anderson, K. S. Detection of novel enzyme intermediates in PEP-utilizing enzymes. *Arch. Biochem. Biophys.* **433** 47–58 (2005).
81. Yoshida, S. et al. A bacterium that degrades and assimilates poly(ethylene terephthalate). *Science* **1979**(351), 1196–1199 (2016).
82. Maity, W., Maity, S., Bera, S. & Roy, A. Emerging roles of PETase and MHETase in the biodegradation of plastic wastes. *Appl. Biochem. Biotechnol.* **193**, 2699–2716 (2021).
83. dos Santos, A. M., da Costa, C. H. S., Silva, P. H. A., Skaf, M. S. & Lameira, J. Exploring the reaction mechanism of polyethylene terephthalate biodegradation through QM/MM approach. *J. Phys. Chem. B* **128**, 7486–7499 (2024).
84. Sevilla, M. E. et al. Degradation of PET bottles by an engineered *Ideonella sakaiensis* PETase. *Polymers* **15**, 1779 (2023).
85. Liu, B. et al. Protein crystallography and site-direct mutagenesis analysis of the poly(Ethylene terephthalate) hydrolase petase from *Ideonella sakaiensis*. *ChemBioChem* **19**, 1471–1475 (2018).
86. Chen, S., Wu, Y., Su, L. & Wu, J. Contribution of disulfide bond to the stability of *Thermobifida fusca* cutinase. *Food Biosci.* **27**, 6–10 (2019).
87. Tanasupawat, S., Takehana, T., Yoshida, S., Hiraga, K. & Oda, K. *Ideonella sakaiensis* sp. nov, isolated from a microbial consortium that degrades poly(ethylene terephthalate). *Int. J. Syst. Evol. Microbiol.* **66**, 2813–2818 (2016).
88. Palm, G. J. et al. Structure of the plastic-degrading *Ideonella sakaiensis* MHETase bound to a substrate. *Nat. Commun.* **10**, 1717 (2019).
89. Longhi, S. & Cambillau, C. Structure-activity of cutinase, a small lipolytic enzyme. *Biochim. Biophys. Acta (BBA) Mol. Cell Biol. Lipids* **1441**, 185–196 (1999).
90. Matak, M. Y. & Moghaddam, M. E. The role of short-range Cys171–Cys178 disulfide bond in maintaining cutinase active site integrity: A molecular dynamics simulation. *Biochem. Biophys. Res. Commun.* **390**, 201–204 (2009).
91. Fährholz, R. et al. ProteinsPlus: A web portal for structure analysis of macromolecules. *Nucl. Acids Res.* **45**, W337–W343 (2017).
92. Schöning-Stierand, K. et al. ProteinsPlus: Interactive analysis of protein–ligand binding interfaces. *Nucl. Acids Res.* **48**, W48–W53 (2020).
93. Graef, J., Ehrt, C. & Rarey, M. Binding site detection remastered: Enabling fast, robust, and reliable binding site detection and descriptor calculation with DoGSite3. *J. Chem. Inf. Model.* **63**, 3128–3137 (2023).
94. Diedrich, K., Graef, J., Schöning-Stierand, K. & Rarey, M. GeoMine: Interactive pattern mining of protein–ligand interfaces in the Protein Data Bank. *Bioinformatics* **37**, 424–425 (2021).
95. Magalhães, R. P., Cunha, J. M. & Sousa, S. F. Perspectives on the role of enzymatic biocatalysis for the degradation of plastic PET. *Int. J. Mol. Sci.* **22**, 11257 (2021).

Acknowledgements

The authors would like to thank Fundação Amazônica de Amparo a Estudos e Pesquisas (FAPESPA) and Coordenação de Aperfeiçoamento de Pessoal de Nível Superior (CAPES) for their financial support (073/2023) to improve the quality of this research; Pro-Reitoria de Pesquisa e Pós-Graduação (PROPESP/UFPa) for the financial support (PAPQ/2023); the Laboratorio Nacional de Computação Científica (LNCC) and Centro de Computação de Alto Desempenho (CCAD), for providing the supercomputing facilities. J.R.A.S. and J.L. thanks the CNPq funding agency for providing the grants 304610/2023-2, 440053/2022-6, 402141/2023-7, 305182/2021-8 and 402311/2024-8.

Author contributions

Conceptualization, J.L. and M.V.D.O.; methodology, M.V.D.O., G.C., C.H.S.C., C.G.S.S. and J.L.; formal analysis, J.R.A.S.. M.V.D.O., G.C., C.H.S.C., C.G.S.S. and J.L.; investigation, M.V.D.O., G.C., C.H.S.C., C.G.S.S. ; software, M.V.D.O., G.C., C.H.S.C., C.G.S.S. ; data curation, writing—original draft preparation, M.V.D.O., C.N.A., J.R.A.S., A.H.L. and J.L.; writing, review and editing, M.V.D.O., C.N.A., J.R.A.S., A.H.L. and J.L.; visualization, M.V.D.O., C.N.A., J.R.A.S., A.H.L. and J.L.; project administration, J.L.; funding acquisition, J.L. All authors have read and agreed to the published version of the manuscript.

Declarations

Competing interests

The authors declare no competing interests.

Additional information

Supplementary Information The online version contains supplementary material available at <https://doi.org/10.1038/s41598-024-84718-0>.

Correspondence and requests for materials should be addressed to G.C. or J.L.

Reprints and permissions information is available at www.nature.com/reprints.

Publisher's note Springer Nature remains neutral with regard to jurisdictional claims in published maps and institutional affiliations.

Open Access This article is licensed under a Creative Commons Attribution-NonCommercial-NoDerivatives 4.0 International License, which permits any non-commercial use, sharing, distribution and reproduction in any medium or format, as long as you give appropriate credit to the original author(s) and the source, provide a link to the Creative Commons licence, and indicate if you modified the licensed material. You do not have permission under this licence to share adapted material derived from this article or parts of it. The images or other third party material in this article are included in the article's Creative Commons licence, unless indicated otherwise in a credit line to the material. If material is not included in the article's Creative Commons licence and your intended use is not permitted by statutory regulation or exceeds the permitted use, you will need to obtain permission directly from the copyright holder. To view a copy of this licence, visit <http://creativecommons.org/licenses/by-nc-nd/4.0/>.

© The Author(s) 2024